Analytical Optimization of a DInSAR and GPS Dataset for Derivation of Three-Dimensional Surface Motion

Sergey Samsonov and Kristy Tiampo

***Abstract*—A revised method for derivation of three-dimensional surface motions maps from sparse global positioning system (GPS) measurements and two differential interferometric synthetic aperture radar (DInSAR) interferograms based on a random field theory and Gibbs–Markov random fields equivalency within Bayesian statistical framework is proposed. It is shown that the Gibbs energy function can be optimized analytically in the absence of a neighboring relationship between sites of a regular lattice. Because the problem is well posed, its solution is unique and stable, and additional regularization in the form of smoothness is not required. The proposed algorithm is simple in realization, does not require extensive computer power, and is very quick in execution. The results of inverse computer modeling are presented and show a drastic improvement of accuracy when both GPS and DInSAR data are used.**

***Index Terms*—Bayesian statistic, differential interferometric synthetic aperture radar (DInSAR), global positioning system (GPS), Markov random field (MRF).**

I. Introduction

THE complementary nature of global positioning system (GPS) and differential interferometric synthetic aperture radar (DInSAR) measurements can be utilized successfully in a number of ways. GPS measures three-dimensional (3-D) coordinates of GPS site location with high temporal but low spatial resolution. The best spatial resolution currently achieved is about 25 km for the GEONET network in Japan and 10–25 km for the SCIGN network in some areas of Southern California and generally is limited by high installation cost.[1] DInSAR, on the other hand, measures the total deformation between two acquisition scenes projected on the line-of-site (direction between satellite and point on the ground) with high spatial resolution over a wide area, but low temporal resolution. The best temporal resolution of 35 days suitable for long-term continuous measurements was achieved by ERS1/2 missions between 1992–2005, when not considering tandem pairs with temporal resolution of one day between 1995–2000 which are not suitable for long-term deformation studies but very useful for co-seismic measurements [1].

In [2], a Bayesian statistical approach and Markov random field (MRF) theory [3], [4] were applied to derived high-resolution 3-D surface velocity maps from the GPS and DInSAR data by minimizing the energy function of the corresponding Gibbs random field distribution. According to the Hammersley–Clifford theorem [4] of equivalence, Markov and Gibbs random fields are identical and minimization of the Gibbs energy with respect to its arguments results in true realization of the MRF.

In general, this approach is very effective and can be extended further to account for other available data, such as a second DInSAR interferogram or leveling data. However, the main disadvantage of this method is that it requires a global optimization technique such as simulated annealing. Such methods of global optimization are extremely slow in convergence, even on small grids, and do not guarantee convergence to global minimum [5].

Instead, we propose a slightly different method for derivation of 3-D velocity maps by minimizing the energy function in a similar form, but without the smoothness criteria, and thus without the smoothness term. In general a smoothness criterion is not realistic. Indeed, the surface velocity field in tectonic regions is not continuous everywhere, depending on the horizontal wavelengths of interest. For example, while the long spatial wavelength regional plate motion velocity is inherently smooth in southern California on both long and short temporal scales, in the smaller fault areas it is not due to local effects, which are of greater interest for the joint application of GPS and DInSAR [6], [7]. In general, this smoothness requirement can be replaced by a weaker piecewise smoothness criterion. However, as we will show below in practice it is not necessary, because the initial problem is well posed and can be minimized analytically.

II. Theory

In this section, theoretical aspects of Bayesian statistics and MRF theory are summarized briefly from [4].

Bayesian inference is a theory of fundamental importance in estimation and decision-making. It is based on the Bayes theorem, which relates posterior and prior probabilities according to the following equation:

$$P(f|d) = \frac{P(d|f)P(f)}{P(d)} \propto P(d|f)P(f) \tag{1}$$

Manuscript received May 28, 2005; revised August 16, 2005. This work was supported in part by the Natural Sciences and Engineering Research Council under Discovery Grant and in part by SEG-KEGS and CSEG scholarships received by S. Samsonov. Technical support for this work has been provided by the POLARIS network.

The authors are with the Department of Earth Sciences, University of Western Ontario, London, ON N6A 5B7, Canada (e-mail: ssamsono@uwo.ca).

Digital Object Identifier 10.1109/LGRS.2005.858483

[1]See also K. Hudnut *et al.* "The Southern California Integrated GPS Network (SCIGN)" http://www.scign.org and Y. Hatanaka *et al.* "GPS meteorology project in Japan" http://dbx.cr.chiba-u.jp.

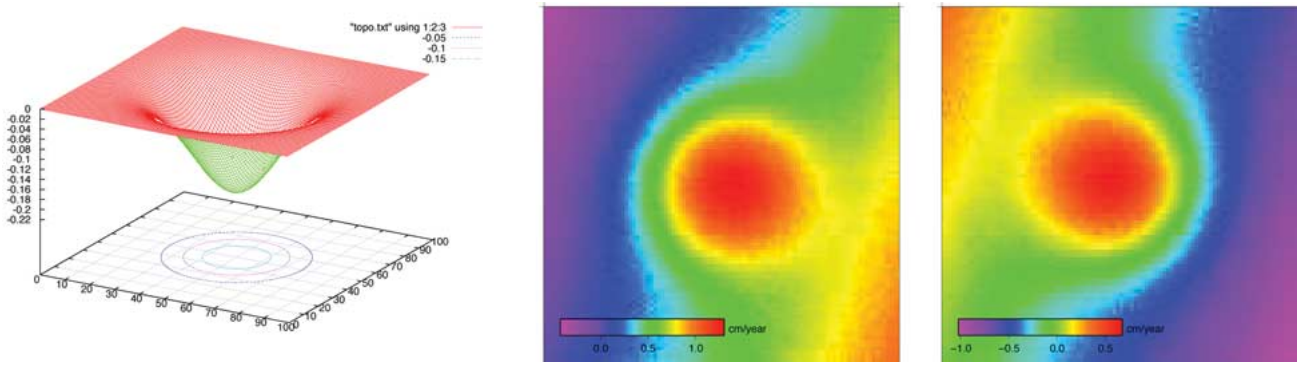

Fig. 1. Computer-simulated data. (a) Topography of the simulation used for modeling. (b), (c) Two DInSAR interferograms calculated from synthetic data which then are used for GPS DInSAR optimization. (a) Topography of the simulation. (b) DinSar interferogram calculated for $(S_x, S_y, S_z) = (0.34, -0.095, 0.935)$. (c) DInSar interferogram calculated for $(S_x, S_y, S_z) = (-0.34, 0.095, 0.935)$.

where $P(f|d)$ is the posterior distribution, $P(f)$ is the prior distribution, $P(d|f)$ is the conditional probability or the *likelihood* of the observation d, and $P(d)$ is the density of d which is constant when d is given and therefore can be skipped in the future derivations.

In Bayes estimation, a risk is minimized to obtain the optimal estimate. The Bayes risk of estimate f^* is defined as

$$R(f^*) = \int_{f \in F} C(f^*, f) P(f|d) df \tag{2}$$

where $C(f^*, f)$ is a cost function defined as

$$C(f^*, f) = \begin{cases} 0, & \text{if } \|f^* - f\| \le \delta \\ 1, & \text{otherwise} \end{cases} \tag{3}$$

where δ is any small constant.

The Bayes risk can be calculated by substitution of (3) in (2)

$$\begin{aligned} R(f^*) &= \int_{f:\|f^*-f\|>\delta} P(f|d) df \\ &= 1 - \int_{f:\|f^*-f\|\le\delta} P(f|d) df. \end{aligned} \tag{4}$$

As $\delta \to 0$ the above equation can be approximated by the following:

$$R(f^*) = 1 - \kappa P(f|d) df \tag{5}$$

where κ is the volume of the space containing all points for which $\|f^* - f\| \le \delta$. Therefore, the minimization of (5) is equivalent to maximization of $P(f|d)$.

The posterior distribution $P(f|d)$ can be calculated from the prior distribution and likelihoods in a way given by Bayes theorem (1). The prior distribution can be presented according to the Hammersley–Clifford theorem in a form

$$P(f) = \frac{1}{Z} e^{-U(f)/T} \tag{6}$$

where U is the energy function of corresponding Gibbs random field and

$$Z = \sum_{f \in F} e^{-U(f)/T} \tag{7}$$

is a normalization constant called *partitioning function* and T is a *temperature* which is assumed to be equal to one and skipped in later derivations. Then likelihoods can be calculated in a similar way by

$$p(d|f) = \frac{1}{\prod_{i=1}^{N} \sqrt{2\pi\sigma_i^2}} e^{-U(d|f)} \tag{8}$$

where the energy function is

$$U(d|f) = \sum_{i=1}^{N} \frac{(f_i - d_i)^2}{2\sigma_i^2}. \tag{9}$$

Therefore, the total energy function now can be rewritten in the following form:

$$\begin{aligned} U(f|d) &= U(d|f) + U(f) \\ &= \sum_{i=1}^{N} \frac{(f_i - d_i)^2}{2\sigma_i^2} + U(f). \end{aligned} \tag{10}$$

III. Model

Our goal is to calculate three components of the velocity vector at each grid point from three known datasets: ascending and descending DInSAR interferograms and GPS velocities at the sparse locations. In order to solve this problem the correct Gibbs energy function must be constructed.

The prior distribution $U(f)$ of (10) is the initial assumption about our model, which in general may be correct or incorrect. If the assumption is incorrect and thus carries some misleading information then the posterior distribution will be misleading also, at least in part. Therefore, since the accuracy of initial assumptions is unknown here, we propose not to use it and draw all information from the data only.

Two DInSAR interferograms can be related to components of the velocity vector according to the following equations:

$$\begin{aligned} V_{\text{LOS}}^{1i} &= \left[v_x^i, v_y^i, v_z^i\right] \left[S_x^1, S_y^1, S_z^1\right]^T \\ V_{\text{LOS}}^{2i} &= \left[v_x^i, v_y^i, v_z^i\right] \left[S_x^2, S_y^2, S_z^2\right]^T \end{aligned} \tag{11}$$

where V_{LOS}^{1i} and V_{LOS}^{2i} are the known interferograms defined on a grid of N points, $\left[v_x^i, v_y^i, v_z^i\right]$ are unknown components of

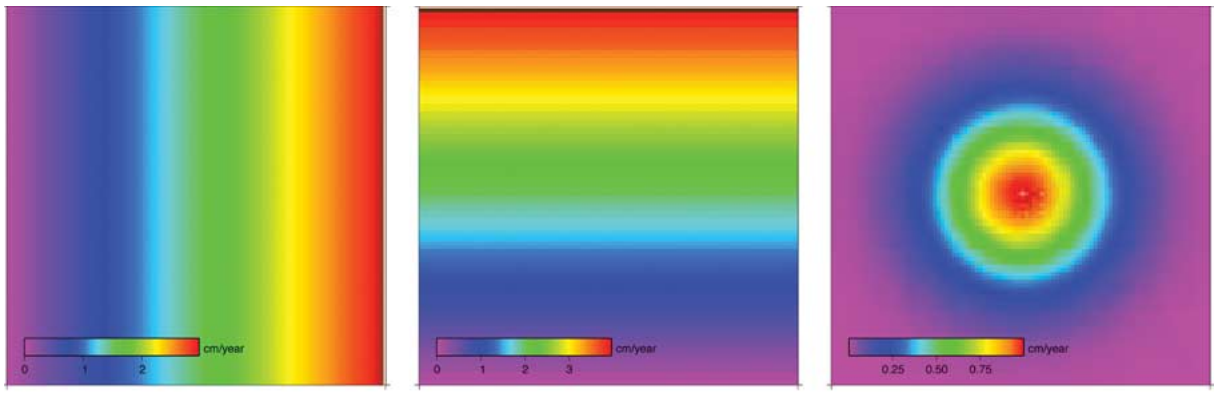

(a) Original v_x component of velocity (b) Original v_y component of velocity (c) Original v_z component of velocity

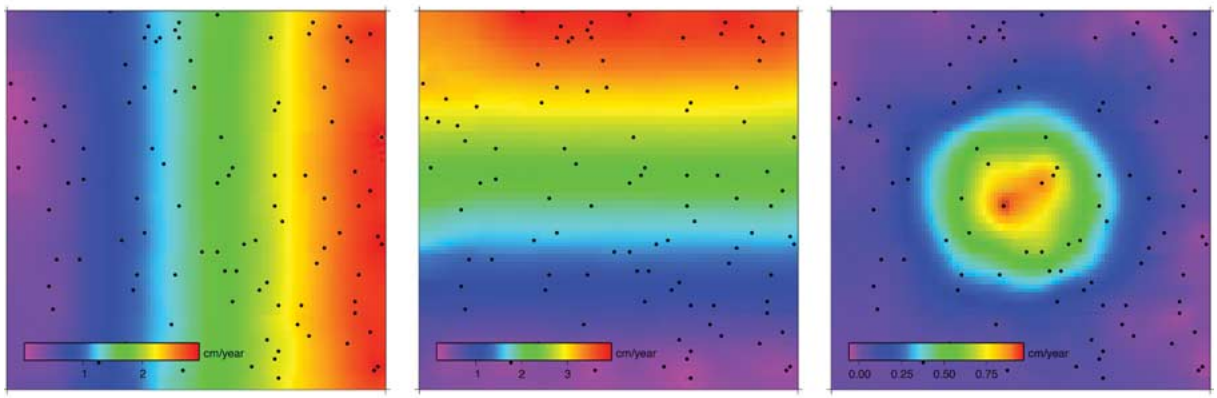

(d) Kriged GPS v_x component of velocity (e) Kriged GPS v_y component of velocity (f) Kriged GPS v_z component of velocity

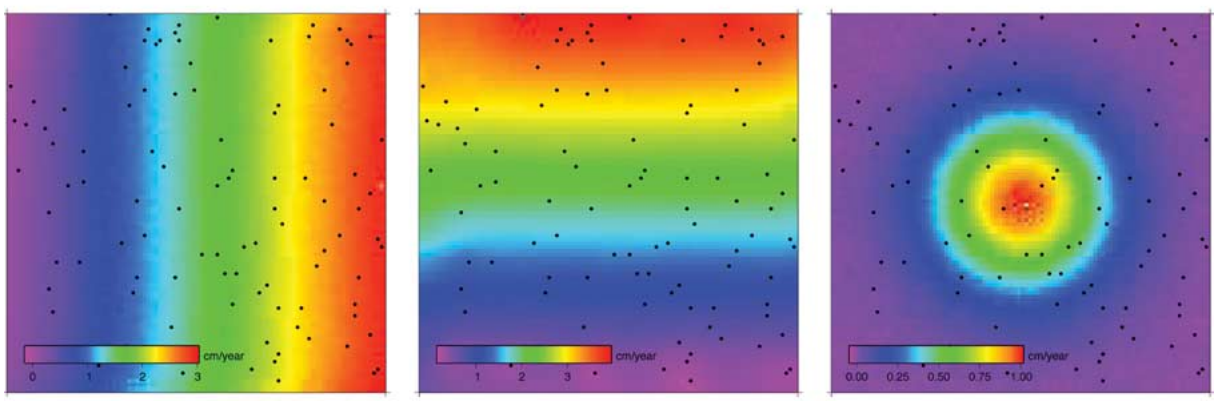

(g) Kriged GPS+DInSAR v_x component of velocity (h) Kriged GPS+DInSAR v_y component of velocity (i) Kriged GPS+DInSAR v_z component of velocity

Fig. 2. Results of computer simulations on 100 × 100 grid. Randomly picked locations (black dots) of 100 GPS stations (same for all plots). (a)–(c) Original modeled components of surface velocity field that are to be restored. (d)–(f) Components of the velocity field interpolated from sparse GPS locations by ordinary kriging. (g)–(i) Restored components of the velocity field after applying GPS-DInSAR optimization. (a) Original v_x component of velocity. (b) Original v_y component of velocity. (c) Original v_z component of velocity. (d) Kriged GPS v_x component of velocity. (e) Kriged GPS v_y component of velocity. (f) Kriged GPS v_z component of velocity. (g) Kriged GPS+DInSAR v_x component of velocity. (h) Kriged GPS+DInSAR v_y component of velocity. (i) Kriged GPS+DInSAR v_z component of velocity.

the velocity vector and $\left[S_x^1, S_y^1, S_z^1\right]$ and $\left[S_x^2, S_y^2, S_z^2\right]$ are unit vectors pointing from the ground toward the satellite.

The GPS velocities are known only at a few sparse locations

$$V^i = \left[V_x^i, V_y^i, V_z^i\right]. \tag{12}$$

Some interpolation technique such as kriging must be used in order to fill in GPS velocities at the DInSAR grid points. Kriging is a method of interpolation which predicts unknown values from data observed at known locations. This method uses a variogram to express the spatial variation, and it minimizes the error

of predicted values which are estimated by spatial distribution of the predicted values [8], [9].

The Gibbs energy function can be rewritten in the following form, where the first two terms correspond to DInSAR and the last three terms correspond to GPS

$$\begin{aligned} u(v_x, v_y, v_z) = \sum_{i=1}^{N} \Big\{ & C_{\text{ins}}^{1i} \left(V_{\text{LOS}}^{1i} - S_x^1 v_x^i - S_y^1 v_y^i - S_z^1 v_z^i \right)^2 \\ & + C_{\text{ins}}^{2i} \left(V_{\text{LOS}}^{2i} - S_x^2 v_x^i - S_y^2 v_y^i - S_z^2 v_z^i \right)^2 \\ & + C_x^i \left(V_x^i - v_x^i \right)^2 + C_y^i \left(V_y^i - v_y^i \right)^2 \\ & + C_z^i \left(V_z^i - v_z^i \right)^2 \Big\} \end{aligned} \tag{13}$$

with coefficients

$$\begin{aligned} C_{\text{ins}}^{1i} &= \frac{1}{2\left(\sigma_{\text{ins}}^{1i}\right)^2} \quad C_{\text{ins}}^{2i} = \frac{1}{2\left(\sigma_{\text{ins}}^{2i}\right)^2} \quad C_x^i = \frac{1}{2\left(\sigma_x^i\right)^2} \\ C_y^i &= \frac{1}{2\left(\sigma_y^i\right)^2} \quad C_z^i = \frac{1}{2\left(\sigma_z^i\right)^2} \end{aligned} \tag{14}$$

where σ's are standard deviations of the measurements.

Equation (13) is a function of $3 \times N$ variables $\left[v_x^i, v_y^i, v_z^i\right]$ where N is the number of grid points. It consists of N nonnegative terms corresponding to the same index i. Therefore, the function $u(v_x, v_y, v_z)$ reaches its global minimum when each subgroup with the same index i is minimal, and the first partial derivatives $(\partial u/\partial v_x^i)$, $(\partial u/\partial v_y^i)$, $(\partial u/\partial v_z^i)$ are equal to zero

$$\begin{aligned} \frac{\partial u}{\partial v_x^i} = & -2C_{\text{ins}}^{1i} S_x^{1i} \left(V_{\text{LOS}}^i - S_x^{1i} v_x^i - S_y^{1i} v_y^i - S_z^{1i} v_z^i \right) \\ & - 2C_{\text{ins}}^{2i} S_x^{2i} \left(V_{\text{LOS}}^i - S_x^{2i} v_x^i - S_y^{2i} v_y^i - S_z^{2i} v_z^i \right) \\ & - 2C_x^i \left(V_x^i - v_x^i \right) \\ \frac{\partial u}{\partial v_y^i} = & -2C_{\text{ins}}^{1i} S_y^{1i} \left(V_{\text{LOS}}^i - S_x^{1i} v_x^i - S_y^{1i} v_y^i - S_z^{1i} v_z^i \right) \\ & - 2C_{\text{ins}}^{2i} S_y^{2i} \left(V_{\text{LOS}}^i - S_x^{2i} v_x^i - S_y^{2i} v_y^i - S_z^{2i} v_z^i \right) \\ & - 2C_y^i \left(V_y^i - v_y^i \right) \\ \frac{\partial u}{\partial v_z^i} = & -2C_{\text{ins}}^{1i} S_z^{1i} \left(V_{\text{LOS}}^i - S_x^{1i} v_x^i - S_y^{1i} v_y^i - S_z^{1i} v_z^i \right) \\ & - 2C_{\text{ins}}^{2i} S_z^{2i} \left(V_{\text{LOS}}^i - S_x^{2i} v_x^i - S_y^{2i} v_y^i - S_z^{2i} v_z^i \right) \\ & - 2C_z^i \left(V_z^i - v_z^i \right). \end{aligned} \tag{15}$$

This set of three linear equations with three unknowns can be constructed for each grid point. It is always solvable when the determinant of the matrix of coefficients is not zero. It can be shown that this condition is always true when the coefficients (14) are not zeros. Because this is the case in every instance, the exact analytical solution can be easily calculated. In this example, Gaussian elimination method was used, but is not presented here due to space limitations.

A. Programming Aspect

The solution of the set of (15) is the standard inverse problem of the form $X = A^{-1}\tilde{u}$. Matrix A in this equation is nonsingular and the inverse matrix A^{-1} is continuous on any point where C_x, C_y, C_z are not null at the same time, which occurs in almost all cases. Therefore, a unique, stable solution always exists. However, in numerical calculations, the fact that $\det A$ can become very small when errors are big gives instabilities of the type 0/0 and the limit, which always exists, must be calculated carefully.

IV. Numerical Simulation

The inverse problem was solved on a equally spaced 100×100 two-dimensional grid with the initial topography shown on Fig. 1(a) and given by

$$z(x, y) = z_0 e^{-((x^2+y^2)/w)} \tag{16}$$

where $z(x, y)$ is the elevation at a point $\{x, y\}$, z_0 is the initial maximum (minimum) elevation of the central point, and w is a form-factor used to adjust the slope and the size of the hill.

The surface velocities at each grid point were calculated by the following equations over a period of ten years

$$v(x) = v_x^0 x \quad v(y) = v_y^0 y \quad v(z) = \frac{\partial z(x, y, t)}{\partial t} \tag{17}$$

with $z_0 = at + b\sin(2\pi t)$, where v_x^0, v_y^0, a, and b are constants.

This model is somewhat realistic. The horizontal velocity in $x(y)$ direction is proportional to $x(y)$, which is similar to stretching with a constant strain rate in that direction. The vertical velocity has two components—linear (slow uplift) and periodic, as, for example, a groundwater-related seasonal signal.

Modeling was performed for 12, 25, 50, and 100 GPS sites with randomly selected locations. For each site, three time series of $\{x, y, z\}$ components of the sites location were generated. Gaussian noise of a form $N = (0, \sigma = 0.5\ \text{cm})$ was added to each horizontal component and of form $N = (0, \sigma = 1\ \text{cm})$ to each vertical component of site location. Also two DInSAR images [Fig. 1(b) and (c)] were calculated by (11) with unit vectors pointing from the center of the image (plane wave approximation) to the satellite $[S_x, S_y, S_z] = [0.34, -0.095, 0.935]$ and $[-0.34, 0.095, 0.935]$, and Gaussian noise of the same form $N = (0, \sigma = 0.2\ \text{cm})$ was added. Also, one simulation was done on data with 12 GPS sites without noise added to the interferograms in order to compare the efficiency of the proposed method with the result presented in [2]. The displacements in each grid point of the DInSAR images were divided by timespan between two acquisitions (ten years), therefore converting it from displacement into velocities.

Linear regression was used to calculate the deformation velocity from GPS data. The ordinary kriging subroutine from [9] was used to interpolate GPS velocities on the grid similar to DInSAR. Therefore, three files of kriged v_x, v_y, and v_z velocity components were generated. The two DInSAR images along with kriged GPS data were used to calculate the final velocities by (15).

V. Results

The results of inverse computer modeling are presented in Table I for different number of GPS stations and in Fig. 2 for one particular case of 100 GPS sites.

TABLE I
ROOT MEAN SQUARE ERROR CALCULATED FOR KRIGED GPS AND KRIGED GPS + DINSAR DATASETS (CENTIMETERS PER YEAR)

	v_x	v_y	v_z
	12 GPS Stations (no DInSAR noise)		
Kriged GPS	0.244	0.326	0.113
Kriged GPS + DInSAR	0.087	0.310	0.0001
	12 GPS Stations		
Kriged GPS	0.244	0.326	0.113
Kriged GPS + DInSAR	0.093	0.310	0.015
	25 GPS Stations		
Kriged GPS	0.238	0.284	0.098
Kriged GPS + DInSAR	0.080	0.267	0.015
	50 GPS Stations		
Kriged GPS	0.124	0.114	0.077
Kriged GPS + DInSAR	0.041	0.096	0.015
	100 GPS Stations		
Kriged GPS	0.081	0.104	0.033
Kriged GPS + DInSAR	0.040	0.098	0.015

The original velocity field which was used to simulate GPS and DInSAR data is presented in Fig. 2(a)–(c). The horizontal velocity field is gradual and ranging from 0 cm/year at the origin to 3 cm/year for v_x and 4 cm/year for v_y components. The vertical component v_z of velocity is gradual at the periphery but very steep at the center of the area, where it reaches $1 \pm 0.5\ \mathrm{cm/year}$. GPS sites coverage is not uniform and a few areas with lower then average coverage are present.

Fig. 2(d)–(f) represents three velocity components interpolated only by ordinary kriging from sparse GPS data. It is noticeable that the velocity in the areas with high density of GPS is well resolved, especially in its horizontal components. The top and the middle parts of left edge, however, are distorted due to the sparseness of GPS coverage in those areas. The vertical component is resolved better at the periphery, but badly resolved at the center, in this case due to its steepness.

Fig. 2(d)–(f) are the final components of velocity calculated by the proposed GPS DInSAR optimization method. The error analysis is presented in Table I.

The best accuracy improvement is achieved for the vertical v_z component, for which the RMS error 0.015 cm/year is almost constant (up to the third decimal) and does not depend on the number of GPS sites used for kriging. This was expected as both DInSAR images used for reconstruction have vertical directional cosine 0.95 and therefore are particularly sensitive to vertical movement. The computer simulation with 12 GPS sites without DInSAR noise gives a much higher accuracy of 0.0001 cm/year, which suggests that the method is very sensitive to the noise presented in the interferograms.

The worst resolved component is horizontal v_y, for which the RMS error decreased by around 10% only. This is due to the imaging configuration used in this particular modeling. Both ascending and descending interferograms have directional cosine in the y direction equal to ± 0.095 and, therefore, are almost blind to the movement in this direction.

The improvement in accuracy of the v_x component is somewhat intermediate—the RMS decreased by about 2–2.8 times. It is interesting that noise is particularly noticeable on this component; however, it can be eliminated by standard low-pass filtering if necessary.

The result of the computer simulation with only 12 GPS sites is presented, and no noise is added to DInSAR data. This can be approximately compared with the results provided in [2] in Table I. In this work, similar results were presented for the case of 12 GPS stations and one DInSAR interferogram on 164×164 grid, and simulated annealing was used to minimized Gibb's energy function. By the direct comparison of the RMS errors, it is seen that our method provides better improvement in accuracy, especially of the vertical component.

VI. SUMMARY AND CONCLUSION

The accuracy of the computed surface velocity field was increased drastically by applying the proposed GPS-DInSAR optimization technique, in comparison with GPS data alone. The proposed method is efficient and can be applied in regions with sparse or dense GPS coverage. It is simple in realization and does not require powerful computing and large memory spaces since each pixel is processed independently. It is ready to be applied to areas such as California where good GPS coverage is achieved and DInSAR data are available.

It is possible to extend this method to other datasets which are available or will be available in the future such as leveling data and/or, perhaps, DInSAR images taken from different positions or by different satellites.

ACKNOWLEDGMENT

The authors would like to thank Dr. Rasmussen for his comments regarding numerical stability of the proposed method.

REFERENCES

[1] D. Massonnet and K. Feigl, "Radar interferometry and its application to changes in the earth surface," *Rev. Geophys.*, vol. 36, no. 4, pp. 441–500, 1998.
[2] S. Gudmundsson and F. Sigmundsson, "Three-dimensional surface motion maps estimated from combined interferometric synthetic aperture radar and GPS data," *J. Geophys. Res.*, vol. 107, no. B10, 2002.
[3] P. Lee, *Bayesian Statistic, An Introduction*. London, U.K.: Arnold, 1989.
[4] S. Li, *Markov Random Field Modeling in Image Analysis*. Berlin, Germany: Springer-Verlag, 2001.
[5] W. Press, S. Teukolsky, W. Vetterling, and B. Flannery, *Numerical Recipes in C: The Art of Scientific Computing*. Cambridge, U.K.: Cambridge Univ. Press, 1992.
[6] D. Dong, T. Herring, and R. King, "Estimating regional deformation from a combination of space and terrestrial geodetic data," *J. Geodesy*, vol. 72, pp. 200–214, 1998.
[7] K. Watson, Y. Bock, and D. Sandwell, "Satellite interferometric observation of displacements associated with seasonal groundwater in Los Angeles basin," *J. Geophys. Res.*, vol. 107, no. B4, 2002.
[8] P. Brooker, *A Geostatistical Primer*. Singapore: World Scientific, 1991.
[9] C. Deutsch and A. Journel, *GSLIB Geostatistical Software Library and User's Guide*. Oxford, U.K.: Oxford Univ. Press, 1992.